37th UIT Heat Transfer Conference
June, 24-26, 2019, Padova, Italy

Average Friction Factors of choked gas flow in Microtubes

Donghun Kang[1], Chungpyo Hong[1], Danish Rehman[2], Gian Luca Morini[2], Yutaka Asako[3], Mohammad Faghri[4]

Abstract

There A micro-tube passage is a basic and important element in the design of micro heat exchangers and for this reason during the last decade a series of investigations have been made with the aim to clarify the main scaling effects playing an important role in microtubes. In this paper, a combined analysis of numerically and experimentally obtained average friction factors in microtubes under the situation of under-expanded (choked) gas flow is presented. The working fluid (nitrogen) passes through the microtube and discharges into the atmosphere under an increasing inlet pressure. Experiments and numerical computations are performed for microtubes with 249 and 528.9 μm in diameter, by varying the aspect ratio (i.e. length/diameter) from 100 to 200. The numerical methodology to solve the governing equations is based on the Arbitrary-Lagrangian-Eulerian (ALE) method. In order to capture the under-expansion characteristics of the flow during choking, the computational domain is extended in the downstream region beyond the microtube outlet. Both experimental and numerical results were obtained for a wide range of Mach number and Reynolds number. In the previous study, it was demonstrated how the outlet Mach number can be expressed as a function of the tube diameter under choked conditions. In this paper, a data reduction procedure for the estimation of the average friction factor between the inlet and the outlet of the microtube is proposed for choked flows in which the outlet gas temperature and pressure are obtained by using the outlet Mach number calculated numerically as a function of the microtube diameter. It is demonstrated how this data reduction method allows an accurate calculation of the average friction factors in microtubes by using a limited number of parameters which are easy to measure. The results obtained in this way are in good agreement with the numerical predictions as well as with the most common empirical correlations.

[1]Kagoshima University, 1-21-40 Korimoto, Kagoshima, 890-0065 Japan

[2]University Technology Malaysia, Jalan Sultan Yahya Petra 54100 Kuala Lumpur, Malaysia

[3]University of Bologna, Via del Lazzaretto 15/5, 40131 Bologna, Italy

[4]University of Rhode Island, Kingston, RI, 02881, USA

37th UIT Heat Transfer Conference
June, 24-26, 2019, Padova, Italy

Identification of Gas Flow Regimes in Adiabatic Microtubes by means of Wall Temperature Measurements

Ryoji Kashiwagi[1], Chungpyo Hong[1], Yutaka Asako[2], Gian Luca Morini[3], Mohammad Faghri[4]

Abstract

There exists the laminar flow, transitional flow, turbulent flow and choked flow regimes in a microtube gas flow. Development of a non-invasive identification method of the flow regimes within a microdevice is expected. This paper demonstrated how the internal gas flow regimes can be identified by measuring the distribution of the external wall temperature of the microchannel along the flow direction. A series of experiments were conducted by using nitrogen as working fluid through a stainless steel micro-tube with an inner diameter of 523 μm and a fused silica micro-tube having a diameter of 320 μm. The experiments were performed by fixing the back pressure at the exit of the microchannel at the atmospheric value and by varying the inlet pressure in order to modify the gas flow regime. In order to measure the external wall temperature along the microtube, two or three bare type-K thermocouples with a diameter of 50 μm were attached to the micro-tube external surface by using a high conductivity epoxy. In the case of the microtube having a diameter of 523 μm, local pressures were measured at three local pressure ports along the microtube. The pressure ports were placed on the opposite side of the tube wall where three thermocouples were attached (Fig. 1). The microtube external wall was thermally insulated with foamed polystyrene to prevent heat gain or loss from the surrounding. The experimental results show that the wall temperature decreases in the laminar flow regime, increases in the transitional flow regime, decreases in the turbulent flow regime and it stays nearly constants in the choked flow regime. The behavior of the average Fanning friction factor and the local Mach number can be explained by identifying the flow regime. It is clarified that the microtube external wall temperature is a reliable indicator of the flow regime..

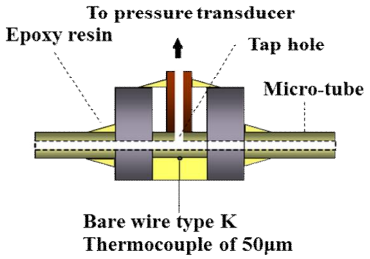

Fig. 1 Details of pressure tap holder

[1]Kagoshima University, 1-21-40 Korimoto, Kagoshima, 890-0065 Japan

[2]University Technology Malaysia, Jalan Sultan Yahya Petra 54100 Kuala Lumpur, Malaysia

[3]University of Bologna, Via del Lazzaretto 15/5, 40131 Bologna, Italy

[4]University of Rhode Island, Kingston, RI, 02881, USA

International Symposium on Thermal Effects in Gas flows In Microscale (ISTEGIM 2019)
October 24-25, 2019, Ettlingen, Germany

Effect of surface roughness on friction Factors of gas flow through micro-tubes

Shuhei Ueda[1], Chungpyo Hong[1], Yutaka Asako[2], Danish Rehman[3], Gian Luca Morini [3]

Abstract

Advanced development to the microfabrication technology has increased the need for an understanding of fluid flow and heat transfer of micro flow devices such as micro-heat exchangers, micro-reactors and many other micro-fluid systems. Therefore, numerous experimental and numerical studies have been performed in an effort to better understand flow characteristics in microchannels. It is well understood that microchannel gas flows are significantly affected by the combined effects of rarefaction (slip on a surface), surface roughness and compressibility. In the present experimental study (Fig. 1), the effects of surface roughness on average and local friction factors of nitrogen gas flow through micro-tubes quantitatively investigated since the effect of surface roughness on micro-channel flows is relatively large compared to conventional tube flows). The $f_{f,\,ave}$ obtained for the glass and the fused silica micro-tube and the $f_{f,\,ave}$ obtained for the stainless steel micro-tube in the range of Re < 5000 coincide with *Blasius* correlation. However, the $f_{f,\,ave}$ obtained for the stainless steel micro-tube deviates from *Blasius* correlation and it coincides with the values obtained by the Colebrook-White equation in the range of Re>7000 because of the effect of the surface roughness (Fig. 2).

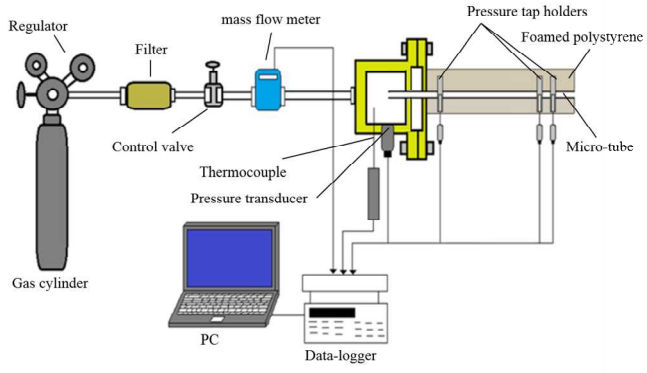

Fig. 1 Schematic of experimental setup

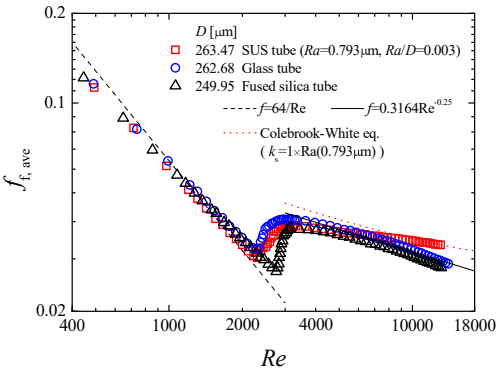

Fig. 2 Average friction factor

[1]Kagoshima University, 1-21-40 Korimoto, Kagoshima, 890-0065 Japan

[2]University Technology Malaysia, Jalan Sultan Yahya Petra 54100 Kuala Lumpur, Malaysia

[3]University of Bologna, Via del Lazzaretto 15/5, 40131 Bologna, Italy

2019 IEEE Wireless Power Transfer Conference,
June 17-21, 2019, London, England

Wide dynamic range rectifier circuit with varactor tuning technique

Ayako Suzuki[1], Koshi Hamano[1], Hayato Shimizu[1], Hiroshi Okazaki[2], Yasunori Suzuki[2], Kunihiro Kawai[2], Atsushi Fukuda[2], Kenjiro Nishikawa[1]

Abstract

This paper proposes and demonstrates a wide dynamic range rectifier with varactor tuning technique. The proposed rectifier employs the tunable device in the input matching circuit, which works to change the impedance matching depending on the input power, resulting in the wide dynamic range operation. The capacity of the varactor as a tuning device changes, as increasing the input power. That adaptively can change the matching circuit to realize the maximum RF-DC conversion efficiency. The proposed prototype rectifier MMIC was fabricated by a commercial 0.25μm GaAs pHEMT process and confirmed the effectiveness of the proposed circuit configuration. The fabricated rectifier MMIC achieves the maximum RF-DC conversion efficiency of 36% at 4.8GHz and 26dBm input power due to the improvement of the matching condition.

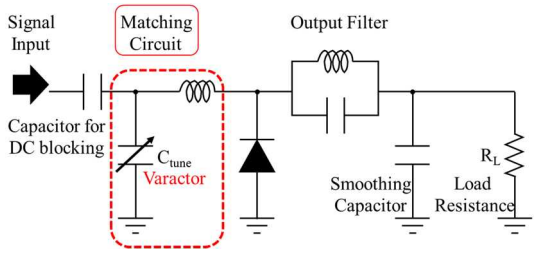

Fig. 1 Configuration of proposed wide dynamic range rectifier.

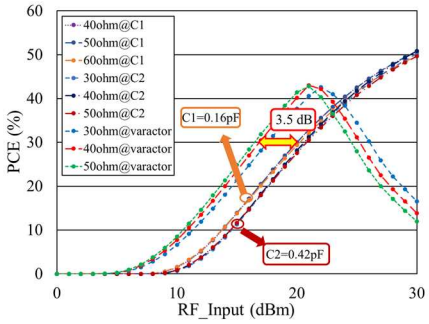

Fig. 2 Rectifier efficiency versus input RF power.

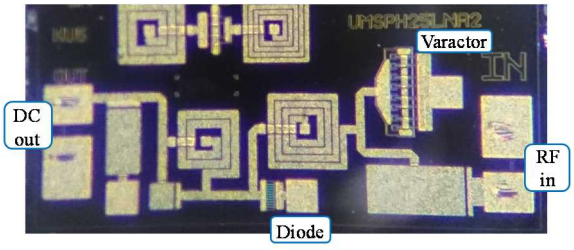

Fig.3 Photograph of fabricated proposed rectifier MMIC.

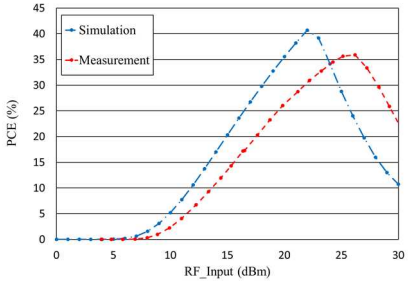

Fig.4 Measured rectifier efficiency.

[1]Department of Electrical and Electronics Engineering, Kagoshima University, Kagoshima, Japan

[2]NTT DOCOMO, INC Kanagawa, Japan

XX International Sol-Gel Conference
August 25-30, 2019, St. Petersburg, Russia

Adhesive properties of water-soluble polysilsesquioxanes containing ammonium, mercapto, and vinyl groups in side-chains

Kento Oshima[1] and Yoshiro Kaneko[1*]

Abstract

The adhesives are mainly classified into drying adhesive, chemical adhesive, and hot-melt adhesive by solidification methods. Although many adhesives have been developed, most adhesives consist of the organic polymers, which can be applied to all types of adhesives described above. Conversely, cement and water glass are practically used as inorganic adhesive, and have properties of excellent heat resistance, durability, and adhesion between inorganic materials. However, because general inorganic materials are poor solubility, "drying adhesive" with excellent storage stability are limited.

So far, we have successfully prepared water-soluble silsesquioxane copolymer containing ammonium and mercapto side-chain groups (**PSQ-AM**), which act as adhesives for inorganic materials such as stainless steels and glasses, by the hydrolytic polycondensation of a mixture of 3-aminopropyltrimethoxysilane (APTMS) and 3-mercaptopropyltrimethoxysilane (MPTMS) using HCl in water/methanol (1:19 v/v) mixed solvent.[1] However, this copolymer could not maintain adhesiveness at 150 °C. It is presumed that **PSQ-AM** could not endure the strain derived from the temperature change in the adherends with different thermal expansion coefficients, *i.e.*, a stainless steel and a glass, because this copolymer has a rigid structure.

Therefore, in this study, slightly flexible structure and loose cross-linked structure were introduced into the aforementioned PSQ to develop inorganic drying adhesives maintaining adhesiveness even at high temperature. To prepare such PSQ, instead of APTMS used in **PSQ-AM** preparation, 3-(2-aminoethylamino)propyltrimethoxysilane (AEAPTMS) as an organotrialkoxysilane containing longer alkyl chain was used. In addition, vinyltrimethoxysilane (VTMS) was also included as a starting material. The hydrolytic polycondensation of a mixture of AEAPTMS, MPTMS, and VTMS was performed using aqueous phosphoric acid (Scheme 1). The resulting terpolymer (**PSQ-2AMV**) was soluble in water. The stainless steel plate and the glass plate adhered using aqueous **PSQ-2AMV** solution were not peeled off even at 200 °C. Moreover, copolymers (**PSQ-2AM** and **PSQ-2AV**) were prepared from AEAPTMS-MPTMS and AEAPTMS-VTMS mixtures, respectively. The stainless steel plate and the glass plate adhered using an aqueous solution of a **PSQ-2AM**-**PSQ-2AV** mixture were also not peeled off at 200 °C.

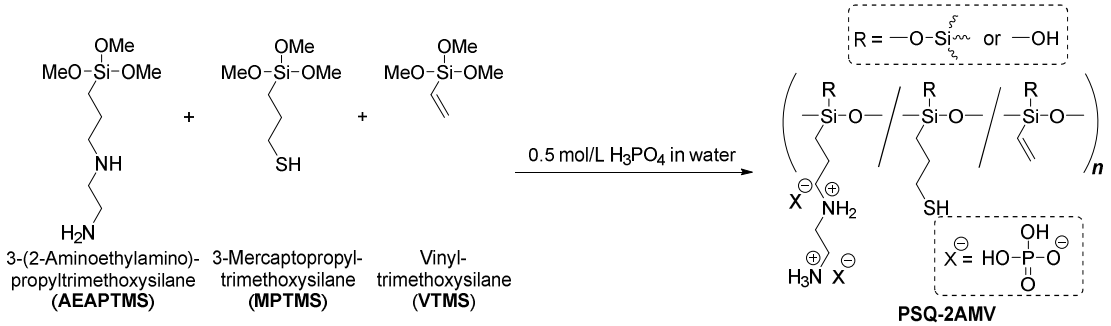

Scheme 1. Preparation of water-soluble PSQ adhesive containing ammonium, mercapto, and vinyl groups in side-chains (**PSQ-2AMV**).

Reference

1. Y. Kaneko, Japanese Patent Application No. 2017-161682 (Aug. 25, 2017)

[1]Graduate School of Science and Engineering, Kagoshima University, 890-0065, Kagoshima, Japan

XX International Sol-Gel Conference,
August 25-30, 2019, St. Petersburg, Russia

Preparation of soluble polyamides by condensation of POSSs containing carboxyl and ammonium groups

Tomoya Kozuma[1] and Yoshiro Kaneko[1]*

Abstract

Polyhedral oligomeric silsesquioxane (POSS) has attracted much attention as an inorganic framework compound with thermal and chemical stabilities and solubility. However, since POSS is an oligomer, it is difficult to apply it alone as film or bulk materials. Therefore, the preparation of POSS-linking polymers has been actively performed in recent years. However, as POSS generally has multiple functional groups, a polymer obtained by its polymerization usually forms a network structure and becomes insoluble. In order to prepare soluble POSS-linking polymers, it is necessary to prepare POSSs in which the number and arrangement of different substituents are controlled.[1,2] However, to prepare such POSSs, complicated reactions and purification processes are required.

Meanwhile, we have reported that POSS-linking polymer can be easily prepared by hydrolytic condensation of a mixture of 3-(2-aminoethylamino)propyltrimethoxysilane and bis[3-(trimethoxysilyl)propyl]amine in a superacid trifluoromethanesulfonic acid aqueous solution.[3] However, this POSS-linking polymer could not form a self-standing film, probably because the alkylammonium group linking POSSs has a flexible structure.

In this study, when an ammonium-group-containing POSS (**Am-POSS**) and a carboxyl-group-containing POSS (**POSS-COOH**), which were previously reported by us,[4,5] were polycondensed using condensing agents, we found that soluble POSS-linking polymer (**POSS Polyamide**) were successfully prepared. Formation of amide bonds was confirmed by FT-IR and ^{1}H NMR measurements. The ^{29}Si NMR spectrum of POSS Polyamide indicated that the POSS structure was maintained even after polymerization. **POSS Polyamide** was soluble in polar solvents, such as water, DMSO, and methanol. In addition, a self-standing film can be formed by heating and evaporating aqueous solution of **POSS Polyamide**.

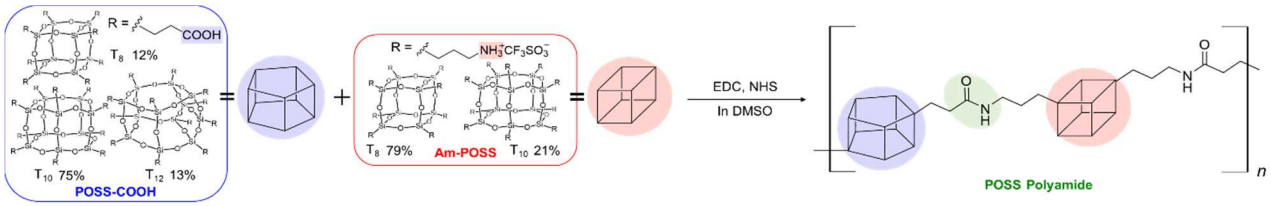

Scheme 1. Preparation of **POSS Polyamide**.

References

1. M. Seino, T. Hayakawa, Y. Ishida, and M. Kakimoto, *Macromolecules*, **2006**, *39*, 3473.
2. T. Maegawa, Y. Irie, H. Fueno, K. Tanaka, and K. Naka, *Chem. Lett.*, **2014**, *43*, 1532.
3. T. Tokunaga, S. Koge, T. Mizuno, J. Ohshita, and Y. Kaneko, *Polym. Chem.*, **2015**, *6*, 3039.
4. Y. Kaneko, M. Shoiriki, and T. Mizumo, *J. Mater. Chem.*, **2012**, *22*, 14475.
5. T. Kozuma, Y. Kaneko, *The Ceramic Society of Japan The 31st Fall Meeting*, (September 2018) 1K22.

[1]Graduate School of Science and Engineering, Kagoshima University, 890-0065, Kagoshima, Japan

XX International Sol-Gel Conference
August 25-30, 2019, St. Petersburg, Russia

Preparation of cationic silsesquioxanes that can stably retain triiodide ion

Ryoya Hasebe[1] and Yoshiro Kaneko[1]*

Abstract

Iodine is known as an excellent dopant (electron acceptor) for improving the conductivity of π-conjugated polymers, such as polyacetylene and polythiophene.[1] However, since iodine is volatile, practical application of iodine-doped π-conjugated polymers indicating high conductivity is difficult. Meanwhile, it has been reported that iodine is stably retained as triiodide ion and/or polyiodide ion in organic polymers, such as starch, polyvinyl alcohol, and a polymer containing imidazolium side-chain groups. Since triiodide ion also functions as an electron acceptor, it may have a possibility as a dopant for π-conjugated polymers. As mentioned above, most of the materials capable of retaining iodine are organic polymers. If iodine can be retained stably with inorganic materials, we believe that the application of materials will expand due to the durability of inorganic materials.

So far, we have found that cationic ladder-like polymeric silsesquioxanes (SQs)[2] and polyhedral oligomeric SQs (POSSs)[3] as soluble inorganic materials were successfully prepared by the hydrolytic condensation of organotrialkoxysilanes containing functional groups convertible to cationic substituents during the reaction.

In this study, we investigated the preparation of cationic SQs capable of stably retaining iodine. Such a SQ could be prepared by hydrolytic condensation (sol-gel reaction) of an imidazolium-funtionalized trialkoxysilane having an iodide counterion in a water/methanol mixed solution of iodine (Scheme 1). Based on UV-Vis and EDX measurements, it was found that this SQ contained triiodide ions. Furthermore, even when this was heated at 100 °C, the content of iodine did not decrease so much. Furthermore, the counterion of imidazolium-group-containing POSS, which was prepared according to our previous report,[4] was converted into triiodide ion. Consequently, even when this product was heated at 100 °C, the triiodide ion was also retained stably.

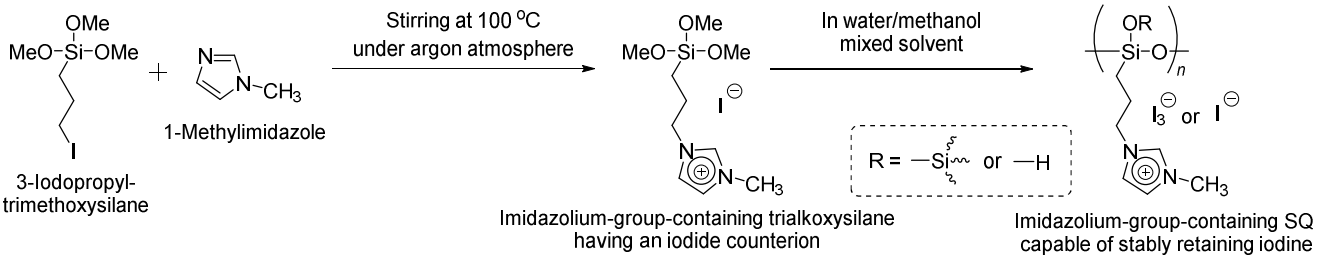

Scheme 1. Preparation of imidazolium-group-containing SQ capable of stably retaining iodine.

References

1. H. Shirakawa, E. J. Louis, and A. G. MacDiarmid, *J. Chern. Phys.*, **1978**, *69*, 5098.
2. Y. Kaneko et al., *Chem. Mater.*, **2004**, *16*, 3417.; *Z. Kristallogr.*, **2007**, *222*, 656.; *Polymer*, **2018**, *144*, 205.
3. Y. Kaneko et al., *J. Mater. Chem.*, **2012**, *22*, 14475.; *J. Mater. Chem. C*, **2014**, *2*, 2496.
4. D. Maeda, T. Ishii, and Y. Kaneko, *Bull. Chem. Soc. Jpn.*, **2018**, *91*, 1112.

[1]Graduate School of Science and Engineering, Kagoshima University, 890-0065, Kagoshima, Japan

XX International Sol-Gel Conference
October 25-30, 2019, St. Petersburg, Russia

Temperature-responsive behavior of POSSs containing ammonium side-chain groups

Takafumi Yoshinaga[1], Yoshiro Kaneko[1]*

Abstract

Most of temperature-responsive materials are organic polymers, *e.g.*, poly(*N*-isopropylacrylamide) (PNIPAM), whereas temperature-responsive oligomers are not common. In particular, to the best of our knowledge, temperature-responsive materials consisting of inorganic oligomers have not been reported. Polyhedral oligomeric silsesquioxanes (POSSs) are cage-like inorganic (siloxane) oligomers, which have thermal and chemical stabilities as inorganic compounds, as well as solubilities as organic compounds. So far, we have reported that ammonium-functionalized POSSs could be prepared by the hydrolytic condensation of amino-group-containing organotrialkoxysilanes using a superacid trifluoromethanesulfonic acid (HOTf) in higher yield with shorter reaction time.[1,2] Furthermore, the effect of the reaction solvents on the preferential formation of crystalline cage-like octamer (T_8-POSS) and amorphous cage-like decamer (T_{10}-POSS) was also investigated.[3,4]

In this study, we found that ammonium-functionalized T_8-POSS with triflate anion (OTf^-) as a counterion (**Am-T8-POSS-OTf**, Figure 1a) in water indicated temperature responsiveness. When aqueous suspension of **Am-T8-POSS-OTf** was heated to 65 °C, it became transparent. Then, when this transparent aqueous solution was cooled to 40 °C, it became turbid (Figure 2). Since these behaviors were observed even after heating and cooling repeatedly, we consider that **Am-T8-POSS-OTf** is regarded as a temperature responsive material.

For comparison, the temperature-responsive properties of ammonium-functionalized T_8-POSS with chloride anion (Cl^-) as a counterion (**Am-T8-POSS-Cl**, Figure 1b) and T_8-POSS (with OTf^- counterion) containing two ammonium groups in the repeating unit (**2Am-T8-POSS-2OTf**, Figure 1c) were also investigated in water by heating and cooling. Consequently, they were transparent at 5–90 °C (Figure 3,4), indicating no temperature responsiveness. Furthermore, when ammonium-functionalized T_{10}-POSS with OTf^- as a counterion (**Am-T10-POSS-OTf**, Figure 1d) was heated and cooled in water, it did not indicate temperature responsiveness (Figure 5).

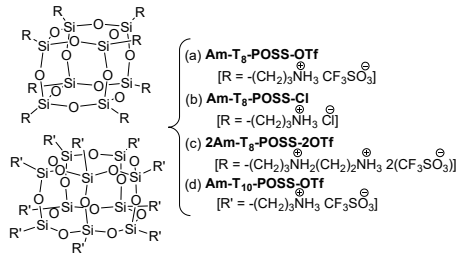

Figure 1. Structures of ammonium-functionalized POSSs.

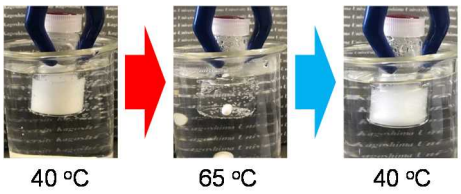

Figure 2. States of **Am-T8-POSS-OTf** in water

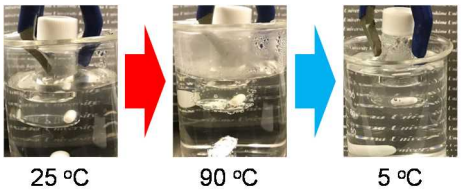

Figure 3. States of **Am-T8-POSS-Cl** in water

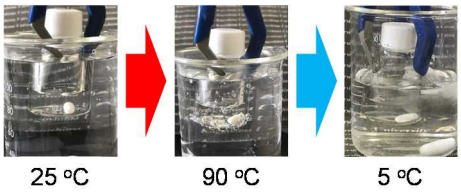

Figure 4. States of **2Am-T8-POSS-2OTf** in water

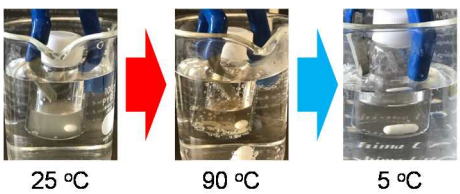

Figure 5. States of **Am-T10-POSS-OTf** in water

References

1. Y. Kaneko, M. Shoiriki, T. Mizumo, *J. Mater. Chem.*, **2012**, *22*, 14475.
2. T. Tokunaga, M. Shoiriki, T. Mizumo, Y. Kaneko, *J. Mater. Chem. C*, **2014**, *2*, 2496.
3. K. Imai, Y. Kaneko, *Inorg. Chem.*, **2017**, *56*, 4133.
4. T. Matsumoto, Y. Kaneko, *Chem. Lett.*, **2018**, *47*, 864.

[1]Graduate School of Science and Engineering, Kagoshima University, JAPAN

The 16th Pacific Polymer Conference (PPC16)

8 – 12 December 2019, Singapore

Dissolution and Composite Preparation of Chitin Using Deep Eutectic Solvents

Satoshi Idenoue[1], Kazuya Yamamoto[1], Jun-ichi Kadokawa[1]

Abstract

Chitin is a natural polysaccharide abundantly present on the earth, and thus, very important biomass resource. However, because it has high crystallinity due to strong intra- and intermolecular hydrogen bonding, its solubility and processability are poor, leading to hardly utilization. On the other hand, ionic liquids have been identified as powerful solvents for polysaccharides with poor solubility. We have already reported that an ionic liquid (IL), 1-allyl-3-methylimidazolium bromide, dissolves chitin in concentrations up to 4.8 wt% [1], but the color of the solution is blacked, owing to the presence of bromide. On the other hand, deep eutectic solvents (DESs), analogs of ILs, are attracting attention as good solvents for natural polysaccharides [2]. In this study, we found that DESs composed of various imidazolium ILs and thiourea as hydrogen bond accepters and donor, respectively, dissolved chitin in 2~5 wt% (Scheme 1) [3]. Furthermore, regeneration of chitin from solutions in AMIMCl/thiourea DES (1:0.5) with additives resulted in the formation of films, which were fabricated from highly entangled nanofibers as the SEM images supported.

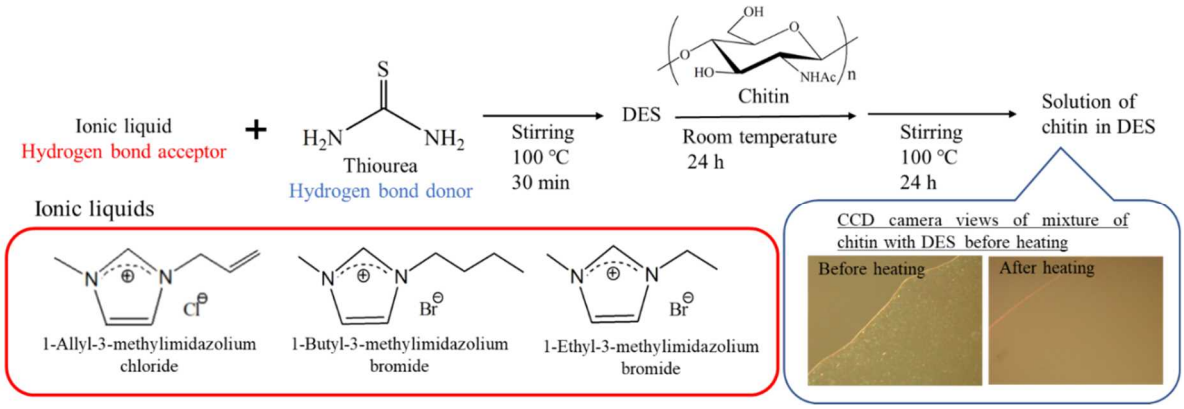

Scheme 1. Dissolution of chitin in DES composed of imidazolium-based ionic liquids and thiourea.

References

[1] K. Prasad, M. Murakami, Y. Kaneko, A. Takada, Y. Nakamura, and J. Kadokawa, *Int. J. Biol. Macromol.,* **2009**, *45*, 221.

[2] M. Sharma, C. Mukesh, D. Mondal, K. Prasad, *RSC Adv*., **2013**, *3*, 18149.

[3] S. Idenoue, K. Yamamoto, J. Kadokawa, *ChemEnineering.*, **2019**, *3*, 90; doi:10.3390/chemengineering3040090.

[1] Department of Chemistry, Biotechnology, and Chemical Engineering, Graduate School of Science and Engineering, Kagoshima University, Kagoshima 890-0065, Japan

The 16th Pacific Polymer Conference (PPC16)

8 – 12 December 2019, Singapore

Preparation of Network Polysaccharides Using Carboxy-terminated Maltooligosaccharide Cross-linker

Hirotaka Chigita[1], Kazuya Yamamoto[1], and Jun-ichi Kadokawa[1]

Abstract

Network polysaccharides are expected as 3D bio-based materials, which have a potential to be applied in biomedical and tissue engineering fields. In this study, carboxy-terminated maltooligosaccharides (GlcA-Glc$_n$-GlcCOONa) were enzymatically synthesized by phosphorylase catalysis and used as cross-linkers to produce network polysaccharides. Phosphorylase catalyzes glucosylation using α-D-glucose 1-phosphate and maltooligosaccharide as glycosyl donor and acceptor, respectively. As this enzyme shows weak specificity for the recognition of the substrate structures, we have already reported that thermostable phosphorylase (from *Aquifex aeolicus* VF5)-catalyzed glucuronylation using α-D-glucuronic acid 1-phosphate as glycosyl donor [1]. In this study, we synthesized GlcA-Glc$_n$-GlcCOONa by the glucuronylation using a maltoheptaose accepter having a carboxylate group at reducing end. Dehydrative condensation between water-soluble chitin (degree of deacetylation: 50 %) and GlcA-Glc$_n$-GlcCOONa was then performed to prepare network polysaccharides, which formed hydrogel in the reaction media **(Scheme 1)**.

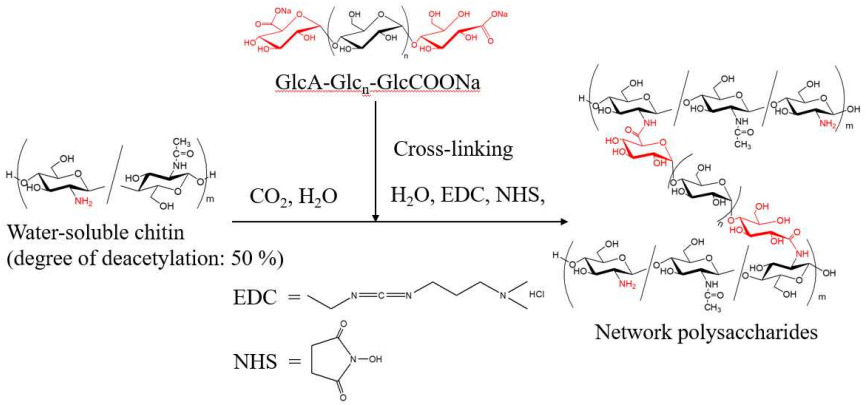

Scheme 1. Dehydrative condensation between water soluble chitin and GlcA-Glc$_n$-GlcCOONa.

References

[1] Y. Umegatani, H. Izawa, M. Nawaji, K. Yamamoto, A. Kubo, M. Yanase, T. Takaha, J. Kadokawa, *Carbohydr. Res.*, **350**, 81 (2012).

[1] Department of Chemistry, Biotechnology, and Chemical Engineering, Graduate School of Science and Engineering, Kagoshima University, Kagoshima 890-0065, Japan

The 16th Pacific Polymer Conference (PPC16)
8 – 12 December 2019, Singapore

Enzymatic Synthesis and Characterization of 2-Deoxyamyloses

Shota Nakamura[1], Kazuya Yamamoto[1], and Jun-ichi Kadokawa[1]

Abstract

Phosphorylase catalyzes enzymatic polymerization of α-D-glucose 1-phosphate (Glc-1-P) as a monomer using a maltooligosaccharide primer to produce α(1→4)-glucan (amylose) [1]. Because of weak specificity for the recognition of substrates, phosphorylase recognizes several analogue substrates of Glc-1-P to give non-natural polysaccharides [2]. Recently, we found that different from potato phosphorylase, thermostable phosphorylase (from *Aquifex aeolicus* VF 5) has ability to recognize D-glucal as a monomer for polymerization. In this study, the synthesis of 2-deoxyamylose was investigated by thermostable phosphorylase-catalyzed enzymatic polymerization of D-glucal via the in-situ production of α-2-deoxy-D-glucose 1-phosphate (2dGlc-1-P) (Scheme 1). The enzymatic copolymerization of D-glucal with Glc-1-P was also carried out. The produced heteropolysaccharide formed a flexible film.

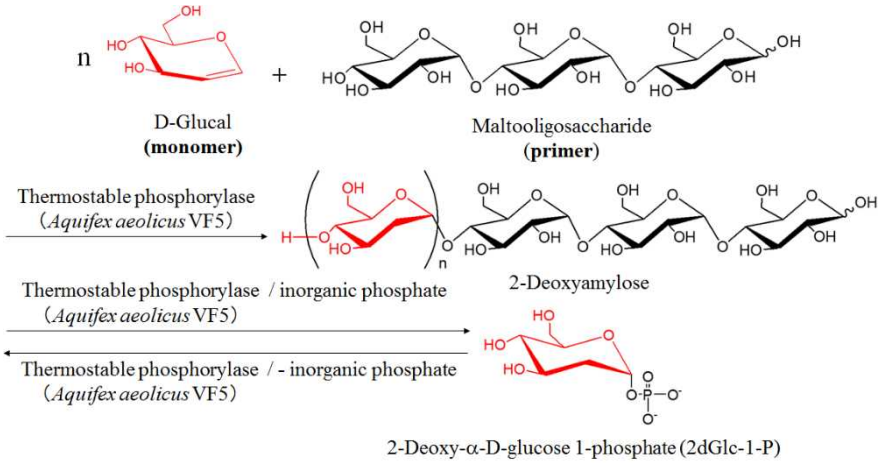

Scheme 1. Thermostable phosphorylase-catalyzed enzymatic polymerization of D-Glucal via in-situ production of 2dGlc-1-P.

References

[1] G. Ziegast, B. Pfannemüller, *Carbohydr. Res.*, **160**, 185 (1987).
[2] J. Kadokawa, *Curr. Org. Chem.*, **21**, 1192 (2017).

[1] Department of Chemistry, Biotechnology, and Chemical Engineering, Graduate School of Science and Engineering, Kagoshima University, Kagoshima 890-0065, Japan

The Pacific Polymer Conference 2019 (PPC16)
8-12, December 2019, Singapore

Preparation of Functional Chitin Nanofiber Composite/hollow Particles by Pickering Emulsion Polymerization

Seiichiro Noguchi[1], Kazuya Yamamoto[1], and Jun-ichi Kadokawa[1]

Abstract

Effective utilization of chitin as the biomass resource has attracted much attention to obtain new bio-based materials. Previously, we reported that the regeneration from a chitin/1-allyl-3-methylimidazolium bromide ion gel using methanol fabricated self-assembled chitin nanofibers. In this study, we performed Pickering emulsion polymerization of styrene using anonic maleyloyl chitin nanofibers as stabilizers. Composite particles were prepared by Pickering emulsion polymerization. We then attempted the conversion of the composite particles into hollow particles by dissolving out inner polystyrene using toluene [1]. The hollow particles were poorly stable when they were re-dispersed in water. To improve stability of hollow particles, in addition to maleyloyl groups, methacryl polymerizable groups were introduced on chitin nanofibers to occur copolymerization with styrene. Hollow particles fabricated by using the bifunctional chitin nanofibers re-dispersed in water while maintaining their morphology. Pyrene, a hydrophobic dye, was encapsulated in cavities of hollow particles by hydrophobic interaction [2]. The encapsulated dye could be released by treatment of the resulting fluorescent hollow particles with surfactant, oleyl alcohol, in water.

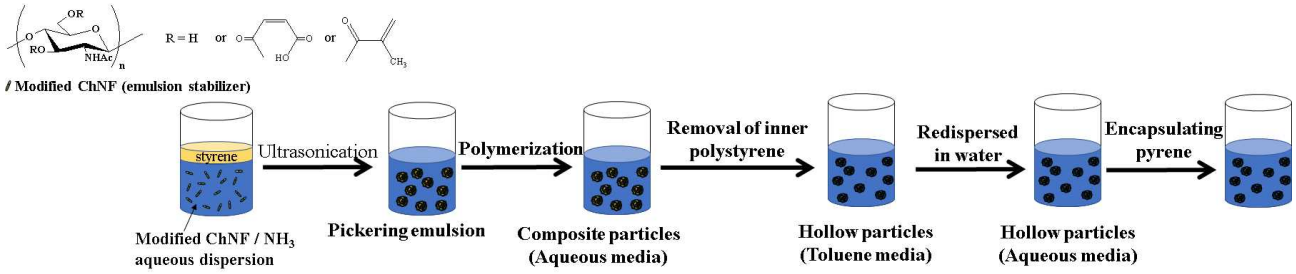

Figure 1. Preparation of functional chitin nanofiber composite/hollow particles by pickering emulsion polymerization.

References

[1] S. Noguchi, K. Sato, K. Yamamoto, J. Kadokawa, *Int. J. Biol. Macromol.*, **126**, 187 (2019).

[2] S. Noguchi, K. Yamamoto, J. Kadokawa, *Int. J. Biol. Macromol.*, in press.

[1] Department of Chemistry, Biotechnology, and Chemical Engineering, Graduate School of Science and Engineering, Kagoshima University, Kagoshima 890-0065, Japan

The 16th Pacific Polymer Conference (PPC16)
8 – 12 December 2019, Singapore

Synthesis and Properties of Mixed Chitin Esters

Hiroki Hirayama[1], Kazuya Yamamoto[1], Jun-ichi Kadokawa[1]

Abstract

Chitin is a natural polysaccharide abundantly present in nature, and thus, very important biomass resource. However, since chitin has strong crystallinity by intermolecular hydrogen bonding between acetamido groups, it is poor in solubility and processability, leading to mostly unutilization. We have already found that 1-allyl-3-metylimidazolium bromide (AMIMBr) dissolves chitin at most in 4.8 wt %. We also found that chitin acylates with high degrees of substitution (DSs) were obtained by acylation of chitin using acyl chlorides in AMIMBr [1]. However, processability of the products was not improved probably due to the remaining hydrogen bonds between acetamido groups. In this study, we synthesized mixed chitin ester having adamantoyl and stearoyl groups in AMIMBr, in which the hydrogen bond would be weaken by introducing bulky and long chain alkyl groups on the chitin chain **(Scheme1)**. The IR and ^{1}H NMR spectra of the product indicated that chitin adamantate stearate with high DS was obtained. In the XRD profile, the diffraction peaks assignable to chitin crystalline structure greatly decreased, and a diffraction peak ascribe to end-to-end packing of stearoyl groups was shown in $2\theta = 3.0°$. The DSC pattern showed an endothermic peak due to enthalpy relaxation of the packing structure at 7 °C. These results suggested that the chitin crystalline structure was disrupted, while the side chain was crystallized. As the product was dissolved in chloroform, the solution could be thinly casted to obtain a flexible film

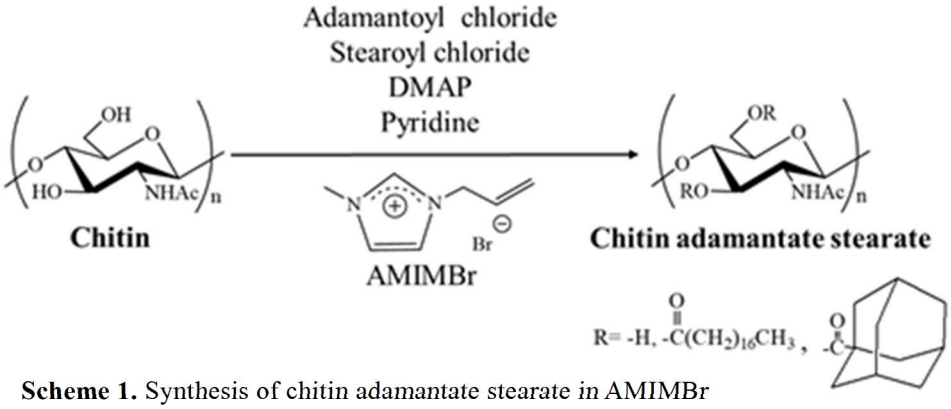

Scheme 1. Synthesis of chitin adamantate stearate in AMIMBr

Reference

1) H. Hirayama, J. Yoshida, K. Yamamoto, J. Kadokawa, *Carbohydr. Polym.* , **200**, 567 (2018).

[1] Department of Chemistry, Biotechnology, and Chemical Engineering, Graduate School of Science and Engineering, Kagoshima University, Kagoshima 890-0065, Japan

Development of fine bubble generator by active control of pressure in gas chamber

Yuma Tsuji, Takashi Goshima*, Kei Mizuta, Susumu Nii
Kagoshima University, Department of Chemical Engineering
*tgoshima@cen.kagoshima-u.ac.jp

Abstract

Fine bubble attracts keen attention and the application is spreading in various fields. Fine bubble is classified into two types of bubbles depending on the size. The larger one is microbubble which is larger than one micrometer and the other is ultrafine bubble which is smaller than one micrometer. Fine bubble is known to promote bacteria culture by increasing the dissolution rate of gas into liquid and to improve washing of solid matters by absorbing dirt materials on gas-liquid interface whose area is extremely large.

Various types of fine bubble generators have been developed upon the requirement of desired bubble size, bubble density at a constant temperature without contamination and of high scalablility without regarding liquid viscosity.

The present study suggests a novel type of generator of fine bubble with high uniformity in bubble size as well as the high bubble density. The key technique of this device is to apply fluidic oscillation inside the nozzle by positive control of pressure fluctuation in the gas chamber.

Bubble size distribution and bubble density were investigated by changing operating parameters. On a specific condition, monodispersed fine bubble with Sauter mean diameter of 84 μm and CV value of 8.5 % was obtained. On the basis of observed values, mechanism of generating fine bubbles in this device would be clarified and the way to enhance bubble density would be discussed.

Key words *: Fine Bubble, Fluidic oscillation, Chamber Pressure, Monodisperse*

Presentation Type: Oral

Titanium hydroxyapatite coating on glass plates and its photocatalyst activity

Ryo Ijichi, Tsutomu Nakazato* and Takami Kai

Abstract

Substances commonly used as solid photocatalysts are titanium oxide TiO_2. However organic adsorption property is generally low. In order to overcome this problem, hydroxyapatite ($Ca_{10}(PO_4)_6(OH)_2$, referred to as HAp) composite[1] and titanium hydroxyapatite, in which a part of the Ca sites of HAp was replaced with Ti ($Ti_xCa_{10-x}(PO_4)_6(OH)_2$, referred to as TiHAp)[2] had been developed to enhance adsorption capacity of TiHAp. As a feature of TiHAp, it is known to have a stronger organic adsorption capacity than TiO_2. Rare earth element containing TiHAp[3], TiHAp and $CaSO_4 \cdot 2H_2O$ with mass ratio 1:1 mixture improved photocatalytic function[4]. Further, as practical examples, a pellet including TiHAp which does not peel off from the pellet surface for water purification application[5], a panel that allows to form a coating layer of easily uniform film thickness that makes it possible to improve the living environment indoors[6].

However, there are limited reports available for water purification using TiHAp as a wall material. The purpose of this study was to clarify the application and hydrophilicity of various powder samples generally exhibiting photocatalytic action, including TiHAp, as wall materials for water purification.

In order to compare the photocatalytic activity under the same conditions, three types of particles were used, namely Titanium Next 21 (TiO_2 0.85%, water 99.15%, Marutomi Co., Ltd.), TiHAp (PHOTHAP PCAP-100, Taihei Chemical Industry Co., Ltd.), TiHAp (Hautoform TA, Fuji Chemical Industry Co., Ltd.) and calcium sulfate dihydrate (Kanto Chemical Co., Ltd.), which does not have photocatalytic function but enhance the photocatalytic effect of TiHAp[4], and using methylene blue (MB) as an adsorbent. Further, ethylsilicate hydrolyzate HAS-1 (SiO_2: 20 wt%, solvent: alcohol, Colcoat Co., Ltd.) was used as a photocatalytic coating agent. Photocatalytic activity was used by photocatalytic evaluation checker. A simple spin coater was used for thin film production. MB solution 400 mg/L (1 mM) was prepared as a standard solution.

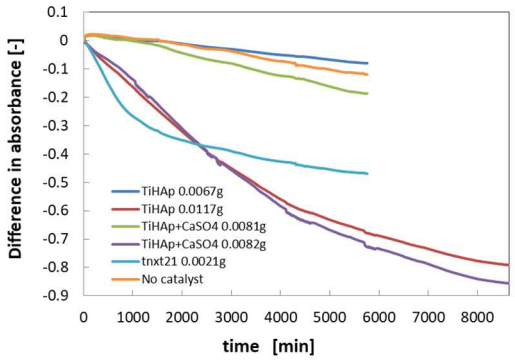

Fig. 1. Results of absorbance measurement of each photocatalyst spin coater coating

Fig. 1 shows the absorbance measurement results of each photocatalyst. TiHAp rapid photocatalytic reaction was observed, titanium next 21 rapid photocatalytic reaction was observed. TiHAp activity was lower than titanium next 21. Titanium next 21 is most active, TiHAp and $CaSO_4 \cdot 2H_2O$ mass ratio 1:1 mixture also showed slightly improved photocatalytic activity. Dependence of photocatalytic activity by the mass of TiHAp was not observed. This is considered to be affected by variations in TiHAp due to spin coaters. Further, it is also conceivable that the accuracy of TiHAp adhesion to the slide glass is not constant in the spin coater. Fig. 2 shows the absorbance measurement results of each photocatalyst. Compared to spin coaters, the difference in changes in the photocatalytic effect was small and stable. From these figure s, the wall material of the photocatalyst coater coating is considered to be excellent.

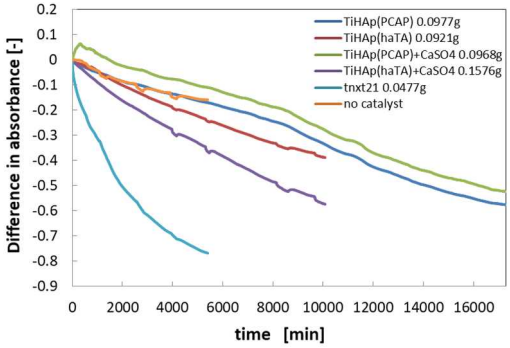

Fig. 2. Results of absorbance measurement of each photocatalyst coater coating

References

(1) S. Ji *et al.*, *Mater. Res. Bull.*, **44**, 768-774 (2009)
(2) M. Wakamura *et al.*, *Langmuir*, **19**, 3428-3431 (2003)
(3) Y. Naganuma *et al.*, Japanese Patent Disclosure 2007-153707 (2007)
(4) T. Nakazato, Japanese Patent Disclosure 2017-189718 (2017)
(5) K. Watanabe *et al.*, Japanese Patent Disclosure 2015-174045 (2015)
(6) H. Yoshida, Japanese Utility Model Registration No. 3202480 (2016)

Department of Chemical Engineering, Kagoshima University, Kagoshima 890-0065, Japan

Production of DMC-biodiesel by alkali heterogeneous catalyst with reduced glycerol by-product

Yuri Ueda, Takami Kai and Tsutomu Nakazato

Abstract

Biodiesel fuel (BDF) has attracted attentions as an alternative fuel for petroleum diesel fuel from the points of resource consumptions and environmental problems caused by the use of fossil fuels. BDF has advantages of renewable, biodegradable and carbon neutral[1]. Conventional BDF is produced by transesterification of vegetable oils and methanol. Glycerol is by-produced by this reaction. The amount of glycerol is about 10 wt% of the products. Because glycerol does not dissolve in BDF, it should be removed from the products[2].

The BDF production method using DMC instead of methanol has been proposed as an alternative method without producing glycerol. The by-products can be dissolved in oil phase and can be used directly as fuel[3]. Several methods of transesterification using DMC have been proposed. The supercritical method has disadvantages such as high temperature and high pressure in the operating condition[4]. The lipase method has disadvantages such as high cost of enzyme and low reaction rate[5]. Alkali catalysts are generally used in the conventional methanol-BDF production. However, because the alkali catalysts do not dissolve in the oil phase containing DMC, a large amount of the catalysts is required to obtain high conversion[6].

We proposed a method using a fine catalyst obtained by dissolving sodium methoxide ($NaOCH_3$) in methanol and then recrystallizing by adding DMC. In this method, we could dramatically reduce the amount of the catalyst[7]. However, this method requires a methanol removal process under reduced pressure. When the methanol removal process is skipped to simplify the process, a small amount of glycerol is produced. However, it is expected glycerol react with DMC to produce glycerol carbonate.

The purpose of this study is to clarify the reaction conditions to obtain high conversion under mild conditions for the production of DMC-BDF with a small amount of methanol, and with reduced glycerol by-production.

Fig. 1 shows the effect of methanol fraction on triglyceride conversion when the catalyst amount to oil was 0.5 wt%. The values on the horizontal axis indicate the methanol fraction considering the stoichiometric ratio in the reaction. The conversion decreased with decreasing the methanol fraction, and has a minimum value. As the increase in the methanol fraction, most of the catalyst dissolved in the methanol phase, and the amount of the fine solid catalyst in the oil phase decreased. When the fraction of methanol increased further, the conversion increased by the transesterification with methanol.

The effect of the catalyst amount is shown in **Fig. 2**. The conversion when the methanol fraction is 0 indicates the result of the reaction by removing methanol under reduced pressure. The addition of a small amount of methanol increased the conversion, and the required amount of the catalyst could be reduced. As shown in **Fig. 2**, the conversion increased or decreased with increasing the methanol fraction in the region where the fraction of methanol was less than 0.2.

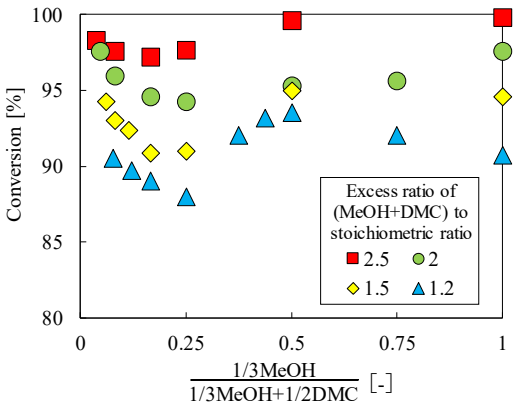

Fig. 1 Effect of methanol fraction on triglyceride conversion (Amount of catalyst = 0.5 wt%)

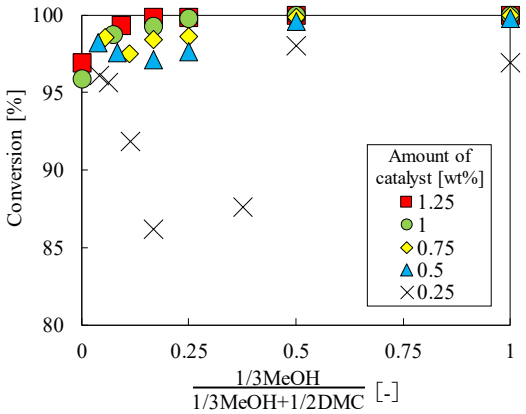

Fig. 2 Effect of methanol fraction on triglyceride conversion (Excess ratio of (MeOH+DMC) to stoichiometric ratio = 2.5)

References

1) Fukuda, H. *et al., Biosci. Bioeng.*, **92**, 405–416 (2001)
2) Dawodu, F. *et al., Renewable Energy*, **68**, 581–587 (2014)
3) Fabbri, D. *et al., Fuel*, **86**, 690–697 (2007)
4) Ang. G. T. *et al., Renew. Sust. Energ. Rev.*, **31**, 61–70 (2014)
5) Tan. K. T. *et al., Fuel*, **89**, 3833–3839 (2010)
6) Zhang, L. *et al., Bioresource Technol.*, **101**, 8144–8150 (2010)
7) Kai, T. *et al., Bioresource Technol.*, **163**, 360–363 (2014)

Department of Chemical Engineering, Kagoshima University, Kagoshima 890-0065, Japan

Production of biodiesel from oils and methyl acetate with alkali heterogeneous catalyst

Sumire Miyajima, Takami Kai, Tsutomu Nakazato

ABSTRACT

Biodiesel fuel (BDF) has attracted attention in view of reduction of fossil fuel consumption, effective utilization of resources and environmental problems. Generally, BDF is produced by the transesterification of vegetable oils with methanol over alkaline catalysts such as potassium methoxide. In this reaction, glycerol with a low purity is by-produced and was usually treated as waste. The BDF production method using methyl acetate (MA) instead of methanol has been reported[1]. Glycerol is not produced in this reaction, and the produced triacetin can be used as an additive for cosmetics, food industry and gasoline. In addition, because the product is homogeneous and all the components can be used as liquid fuel, it is not necessary to separate the product mixture. Supercritical esterification method[1], biocatalyst method[2], and alkaline catalytic method[3, 4] have been studied for the BDF production using methyl acetate. Supercritical method requires conditions such as high temperature and high pressure. The biocatalyst method has disadvantages such as high cost. Alkaline catalytic method requires a large amount of catalysts to obtain high conversion. This is because the alkali catalyst does not dissolve in methyl acetate despite, and the reaction proceeds as a heterogeneous system. In this study, recrystallization method was applied to the esterification with methyl acetate. This method was already applied to the esterification with dimethyl carbonate and the reaction rate could be drastically increased[5]. The reaction conditions to obtain high triglyceride conversion and low alkaline catalyst amount were investigated.

Fig. 1(a) and **(b)** shows the triglyceride conversion after 120 minutes at a temperature of 50°C when the molar fraction of MA in MA and MeOH mixture was changed. The mole ratio of (MA + MeOH) to oil was 4 and 6, and the catalyst amount was 0.25, 0.5, 1.0 wt% to oil. When the mole fraction of MeOH was small and catalyst recrystallization occurred, the conversion was indicated by square symbols. On the other hand, the mole fraction of MeOH was large and all the catalyst dissolved in MeOH, circles were used as symbols.

When all the catalyst dissolved in MeOH, the conversion decreased as the MA ratio increased. The TG conversion at a catalyst amount of 0.25 wt% was low even when the fine catalyst was recrystallized. This is probably because the amount of recrystallized catalyst was not enough for the reaction. When the amount of catalyst exceeded 0.5% by weight, the TG conversion was high even when the molar fraction of MA exceeded 70%.Under these conditions, the catalyst precipitated as fine crystals and dispersed in the oil phase. Therefore, transesterification between MA and oil was promoted. This trend is observed at any molar ratio of (MA + MeOH) to oil, with higher ratios resulting in slightly higher conversions.TG conversion can be dramatically increased by recrystallization methods that produce BDF using methyl acetate.

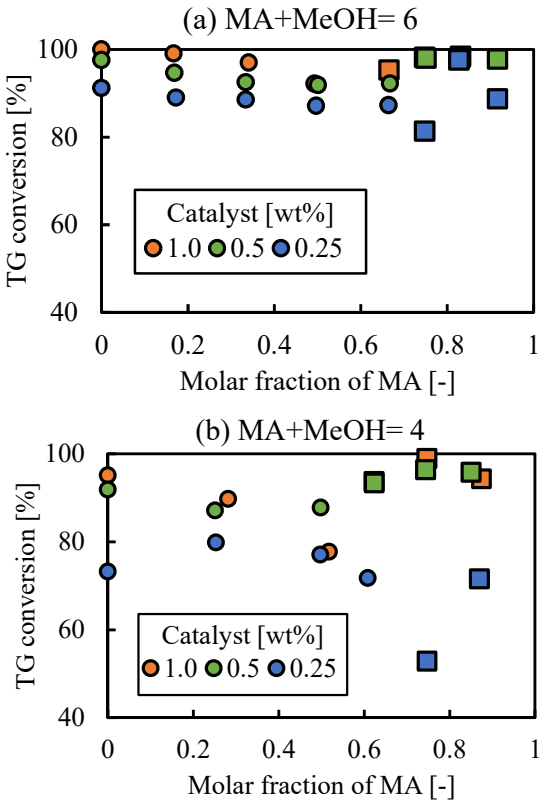

Fig. 1 Effect of molar fraction of methyl acetate on triglyceride conversion

REFERENCES

1) Campanelli, P. *et al*., *Fuel*, **89**, 3675－3682 (2010)
2) Xu, Y. *et al*., B: *Enzymatic*, **32**, 241－245 (2005)
3) Freedman, B. *et al*., *J. Am. Oil Chem. Soc*., **63**, 1375－1380 (1986)
4) Noureddini, H. *et al*., *J. Am. Oil Chem. Soc*., **74**, 1457－1463 (1997)
5) Kai, T. *et al*., *Bioresource Technol*., **163**, 360－363 (2014)

Department of Chemical Engineering, Kagoshima University, Kagoshima 890-0065, Japan

Analysis of defluidization due to gas adsorption by fluidized particles

Yuya Taira, Takami Kai, Tsutomu Nakazato

Abstract

Fluidized beds are widely used in chemical processes. An unexpected decrease in fluidization quality is sometimes observed during the operation of fluidized beds. One of the reasons is that the gas velocity decreases in the emulsion phase. When it decreases below the velocity required for fluidization, the gas drag force becomes too small to balance the gravitational and buoyancy forces acting on the particles. Consequently, the particles agglomerate, resulting in defluidization. In industrial processes, the fluidizing gas is switched at the startup and shutdown of the operation. Defluidization after gas switching was observed when the adsorptivity is higher for the fluidizing gas after the gas switching[1, 2]. Lu *et al.*[3] also reported that pulverized coal particles were not discharged from a hopper when the fluidizing gas was switched from air to CO_2. In this case, defluidization occurred with the decrease in the pressure drop. Understanding the aforementioned phenomena is important when attempting to determine the conditions necessary to maintain good fluidization in industrial processes. In the present study, the effect of the difference in gas adsorptivity on the fluidization behavior was analyzed.

An acrylic resin tube was used for the construction of fluidized bed. The inner diameter and height were 52 mm and 1500 mm, respectively. The settled bed height was 30 cm. A pressure sensor was connected to the port attached to the wall surface of the bottom, and the temporal change of the pressure drop was measured. Activated carbon, porous silica, porous alumina and glass beads were used as fluidizing particles. The first and second fluidizing gases were Ar and CO_2, respectively. They have different adsorption properties, whereas the molecular weight are close. This is because the effect of non-equimolar diffusion[4] due to the difference in molecular weight should be avoided.

In the experiments, Ar gas was supplied at a constant superficial gas velocity. After the stable fluidization was confirmed, the pressure data sampling was started, and the fluidizing gas was switched to CO_2 gas. The pressure drop was recorded and the measurement was finished after confirming that the fluidized state recovered and was stable.

Visualization of the fluidization was performed using a two-dimensional (2D) fluidized bed. Its width and depth of the bed cross section were 130 mm and 5 mm, respectively. The bed was illuminated with back lighting, and the motion of the bed was recorded from the front side of the bed using a video camera. Grayscale values of each image were affected by the intensity of light transmittance. The difference in the particle density in the bed was described graphically by the conversion of grayscale values into colors in the RGB space.

Two types of defluidization phenomena were observed in the case of porous particles. **Fig. 1** shows the temporal change of the fluidization behavior when the fluidizing gas was switched from Ar to CO_2 in a 2D fluidized bed. The superficial gas velocity was 1.5 cm/s for the first gas and 1.9 cm/s for the second gas. The fluidized particles were porous silica with a particle size of 48.7 μm. Fourteen seconds after the fluidizing gas was switched, it can be seen that the emulsion phase aggregated in the bottom of bed and the bed height decreased due to the adsorption of CO_2. The bubbles disappeared after 27 s, and a channel was completely formed. Some of channels were formed. The fluidization restored after 170 s after the channel walls were destroyed by the gas flow. This phenomenon was mainly observed for particles smaller than 100 μm.

Fig. 2 shows the time series of the pictures when the porous silica with 142 μm size was used. The other conditions were the same as those in the experiment represented in Fig. 1. Aggregation of the emulsion phase started immediately after the gas was switched and bubbles completely disappeared, and the whole bed became a fixed bed after 7 s. After 10 s, the bed was plugged by the contracted upper part of the bed. It was lifted by the fluidizing gas. Afterwards, the bottom of this zone gradually collapsed, and fluidization completely recovered after about 80 s. This phenomenon did not depend on the CO_2 adsorption capacity, but was observed for larger particles.

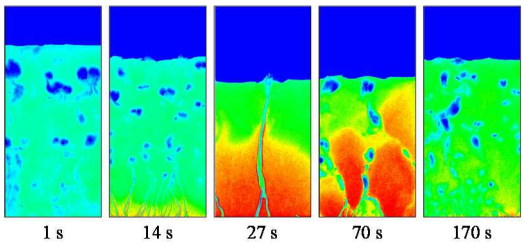

Fig. 1 Channeling behavior after gas switching

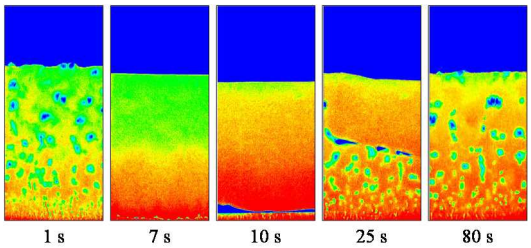

Fig. 2 Plugging behavior after gas switching

References

1) Kai, T., Y. Tashiro, Y. Hirano, T. Nakazato, *Powder Technol.*, **237**, 153–159 (2013)
2) Kai, T., T. Takahashi, *AIChE J.*, **44**, 491–494 (1998)
3) Lu, H., X. Guo, S. Tao, X. Gong, *Powder Technol.*, **281**, 193–199 (2015)
4) Kai, T., K. Terachi, S. Wada, T. Nakazato, *Kagaku Kogaku Ronbunshu,* **44**, 229–235 (2018)

Department of Chemical Engineering, Kagoshima University, Kagoshima 890-0065, Japan

How fine bubbles change germination and initial plant growth of spinach and Japanese mustard spinach

Yudai Mikuni, Takashi Goshima, Kei Mizuta and Susumu Nii*

Department of Chemical Engineering, Kagoshima University
1-21-40, Korimoto, Kagoshima 890-0065, Japan
*niisus@cen.kagoshima-u.ac.jp

Abstract

Fine bubbles, FBs, attract keen attention because of the benefit of enhancing the function of water with less or no use of chemicals. Areas of application rapidly spread to industrial cleaning, pharmaceuticals, material processing, and fishery or plants farming. Among the successful results, the authors paid a special interest on the growth enhancement of plants grown with hydroponic cultivation.

In recent years, the number of fundamental research on working mechanism of FB is growing. Liu et al.[1] reported that enhancement of germination and plant growth in the initial period. They reported that both positive and negative effects appear on various plants. There was an adequate amount of FB depending of the plant species. In this study, we investigated the influence of FB on germination and initial plant growth of spinach and Japanese mustard spinach using oxygen and air UFB in water.

Tap water was chosen as a medium and oxygen or air was dispersed as FBs through a generator that was developed by Goshima, a co-author of this work. The bubble diameter distribution and the number density of UFB were analyzed with Nanosight, LM-10 (Malvern). With and without O_2 and air UFB, germination and subsequent initial growth was examined with fifty seeds of spinach or Japanese mustard spinach. Germination ratio and stem length and root length were observed for comparison. Also, dissolved oxygen concentration in water was measured by DO meter.

The water containing air or O_2 UFB clearly increased the length of the stem length of Japanese mustard spinach by 1.2~1.3 times of that was observed in tap water. Also, the distribution of the stem length was changed by the presence of UFB. Even if the water containing air UFB had low dissolved oxygen, the use clearly promoted the elongation of Japanese mustard stem length. This fact demonstrates that the presence of bubbles improved the plant growth.

[1] S.Liu, et al.;Langmuir, 32(2016)11295-11302

***Key words** : Ultra fine bubbles, Germination, Initial plant growth, Adsorption, Length, Distribution*

Presentation type: Poster, Scientific session: B

The 32st International Symposium on Chemical Engineering, December 6-8, 2019, Daejeon, Korea

Analysis of non-equimolar binary gas diffusion under isobaric condition in molecular diffusion region

Yuta Ochiai, Takami Kai, Tsutomu Nakazato

Abstract

In general, it is recognized that binary gas interdiffusion under isobaric conditions is the equimolar diffusion. It is also known that the diffusion coefficient is inversely proportional to the square root of the molecular weight in the Knudsen diffusion region where the pore size is an order of magnitude smaller than the mean free path of molecules. However, even in the molecular diffusion region where the pore size is orders of magnitude greater than the mean free path, non-equimolar diffusion occurs under isobaric conditions. This phenomenon was initially reported by Graham [1] in 1833. At present, the diffusion rate ratio is expressed by Graham's law, but is not widely recognized.

Although many models have been proposed to explain the mechanism of this phenomenon, all of them are based on the equimolar diffusion coefficients, and attribute the cause to the non-equimolar Knudsen diffusion due to collisions between molecules and walls. Therefore, all the models have not clearly explain Graham's law [2, 3]. Kai [4] proposed a model in which the intrinsic diffusion coefficient for each component was introduced. According to this model, the ratio of the diffusion flux depend on the intrinsic diffusion rate and bulk flow rate caused by the small pressure gradient in the pass. The previous results of many researches under isobaric and isovolumetric systems could be well explained by this model. In this study, the diffusion of hydrogen and argon through a packed bed under isobaric condition was performed using a Wicke-Kallenbach type cell. The upper limit of pore size to cause non-equimolar diffusion was studied.

A diffusion cell was the particle packed bed, and both sides of the cell were connected to the lines in which hydrogen and argon flew separately. The flow rate of the sweep gas was adjusted so that the pressure difference between near both the ends of the diffusion cell became zero. The exit gas composition of each sweep gas was determined by gas chromatography. The carrier gas for gas chromatography was the same gas used as the sweep gas. The average diameter of the glass beads used for the packed bed is 20.7, 63.9, 94.9, 622.3 μm. These values were obtained from the pressure drop using the Kozeny-Carman equation. The temperature of the diffusion cell was kept at 25℃ by circulating water outer surface of the cell.

Fig. 1 shows the measurement results of interdiffusion through a packed bed of particles with an average particle size of 63.9 μm. The ratio of the apparent diffusion coefficients is considered to be approximately equal to the ratio of the apparent diffusion rates (including movement by viscous flow) of each component. In this case, the ratio of the apparent diffusion rates of hydrogen and argon was 3.55. Although this value was rather smaller than 4.45: the calculation from Graham's law, it is obvious that the interdiffusion was not equimolar diffusion. Because the rate of movement is higher for hydrogen than argon, the slight pressure distribution would generate in the packed bed, and allowed the flow in a direction opposite to the movement direction of hydrogen. This caused the reduction of the ratio of the diffusion coefficients of hydrogen to argon.

The steady state diffusion was observed for the other particles having different size. **Fig. 2** shows the relationship between the particle size and the ratio of the apparent diffusion coefficient of hydrogen to argon. As the particle size increased, the ratio of the diffusion coefficients decreased, and approached unity. This is considered to be due to the fact that the rate of viscous flow is larger for large pores (large size of particles) even when the pressure drop is same. The cause of this is unclear, but it may be caused by a slight pressure difference. However, it is considered that non-equimolar diffusion under isobaric conditions occurs in the large pores such as several hundred micrometers.

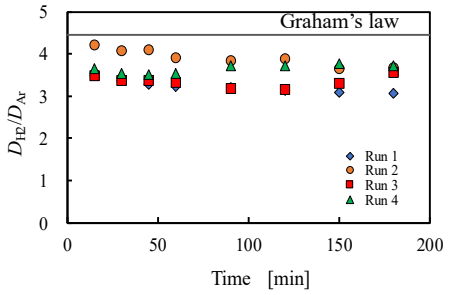

Fig. 1 Temporal change of the ratio of intrinsic diffusion coefficients of H_2 to Ar through the packed bed with 63.9 μm particles

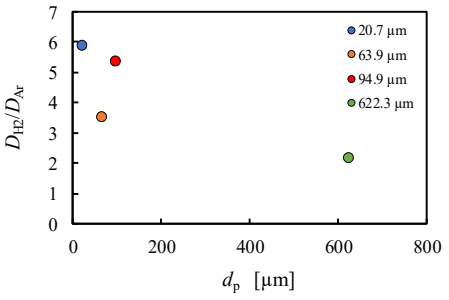

Fig. 2 Effect of packed particle size on the ratio of the apparent diffusion coefficients of H_2 to Ar

References

[1] T. Graham, *Phil. Mag. J. Sci*., **2**, 175–190, 269–276, 351–358 (1833)

[2] A. F. Mills, *Int. J. Heat Mass Tran*., **50**, 5087–5098 (2007)

[3] C. Bao, Z. Jiang, X. Zhang, *J. Power Sources*, **310**, 32–40 (2016)

[4] T. Kai, *Kagaku Kogaku Ronbunshu*, **43**, 271–280 (2017)

Department of Chemical Engineering, Kagoshima University, Kagoshima 890-0065, Japan

Influence of gas properties on bubble behavior in a 3D fluidized catalyst bed

Yuto Fukami, Takami Kai, Tsutomu Nakazato

Abstract

Bubble size is one of the most important parameters in the fluidized bed reactor model. Therefore, many bubble size correlations have been also proposed[1]. However, almost all of these correlations are obtained by experiments using air as the fluidizing gas and Gerdart B particles are used at room temperature. The gas properties are not considered in the correlations. However, in the case of particles classified as Geldart A particles, the expansion rate of the emulsion phase is affected by gas properties[2]. The bubble size is also greatly influenced by the gas properties indirectly[3, 4]. We observed the bubble behavior with various types of gas in a two-dimensional fluidized bed using image analysis[5]. It was confirmed that the voidage of the emulsion phase and bubble behavior was affected by the gas properties. In this study, we measured the frequency of bubbles rising in the bed to clarify the influence of the gas properties on the bubble size in a three-dimensional fluidized bed.

The fluidized bed used in this study is made of acrylic resin that have an inner diameter of 5 cm and a height of 100 cm. Porous silica having a particle diameter of 49 μm and a density of 754 kg/m^3 was used as the fluidized particles. The initial settled bed height was about 30 cm. Argon, carbon dioxide, hydrogen, nitrogen and neon are used as the fluidizing gas. An optical probe having an outer diameter of 1.2 mm was used. The probe was inserted horizontally into the bed, and the bubble frequency was measured by changing the position of the tip in the radial direction and the vertical direction. In order to calculate the bubble size from the bubble frequency measured by the optical probe, the following two assumptions were made: i) the bubble is spherical and has no bubble size distribution, ii) all bubbles passing through the horizontal plane with the tip of the optical probe were detected.

Fig. 1 shows the change in the bubble size based on the bubble frequency with U_G-U_e at a height of 30 cm. The silica particles are fluidized with each gas in the 3D fluidized bed. When the bed was fluidized with hydrogen, the bubble size was the largest and decreased in the order of carbon dioxide, nitrogen, argon and neon. Since it has been reported that the expansion ratio of the emulsion phase is inversely proportional to the gas viscosity and density to the power of 0.12. The bubble size decreased with increasing the parameter. It is confirmed that the emulsion phase voidage was small and the bubble size was large when hydrogen was the fluidizing gas in a 2D fluidized bed. Thus, the gas properties affect the expansion ratio of the emulsion phase, and finally affect the bubble size. We directly observed[6] the bubble size in a 2D fluidized bed Because the depth was very small, bubble growth was probably influenced by the friction by the walls. The bubble size in the 2D fluidized bed was much smaller than that in the 3D fluidized bed. In order to confirm the relationship between the gas properties and the bubble size, the result in the 3D fluidized bed was compared with that in the 2D fluidized bed in **Fig. 2** The horizontal axis is the bubble size in the 2D fluidized bed, and the vertical axis is the bubble size in the 3D fluidized bed. The same particles were fluidized, and the bubble size were measured at 0.15 m height for both of them. Although the bubble size in the 3D fluidized bed was much larger than that in the 2D fluidized bed, it can be seen that the effect of the gas properties on the bubble size was almost the same for both the fluidized bed.

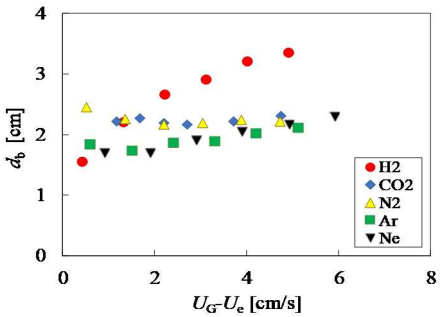

Fig. 1 Effect of gas type and gas velocity on bubble size; L = 30 cm.

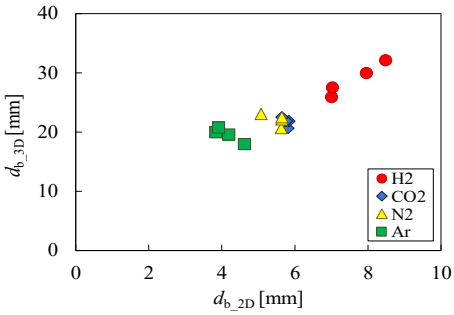

Fig. 2 Comparison of bubble size measured in a 2D-fluidized bed and in a 3D-fluidized bed.

References

1) Karimipouret, S. *et al*., *Powder Technol*., **205**, 1–14 (2011).
2) Abrahamsen, A.R. *et al*., *Powder Technol.*, 26, 47–55 (1980).
3) Kai, T. *et al*., *J. Chem. Eng. Japan*, **19**, 67–71 (1986).
4) Kai, T. *et al*., *Powder Technol*., **51**, 267–271 (1987).
5) Hiromori, Y. *et al*., Preprint 24th SCEJ Symp. Fluidization & Particle Processing, Hachioji, Dec. 5-7, 97–100 (2018).

Department of Chemical Engineering, Kagoshima University, Kagoshima 890-0065, Japan

The 32st International Symposium on Chemical Engineering, December 6-8, 2019, Daejeon, Korea

Influence of gas volume expansion in a fluidized catalyst bed on bubble behavior

Junya Shingu, Takami Kai, Tsutomu Nakazato

Abstract

Fluidized catalyst beds have been applied to many chemical processes since they were used in an FCC process. In the fluidized catalyst bed, reactions mainly occurs in the emulsion phase in which most of the catalyst particles exist. Therefore, it is important to increase the mass transfer rate between the bubbles and the emulsion phase. Since the interfacial area of the bubbles directly affects the mass transfer rate, it is important to generate small bubbles. A reactor model is required for the design of the fluidized bed reactor. Since the bubble size is an important parameter in the model, many researchers have studied the characteristics of the bubbles and have found knowledge of derived an understanding of the bubble behavior. Many correlations for bubble size estimation have also been reported[1]. Bubble size will be affected by temperature, pressure, gas properties and gas volume change. A gas volume change is stoichiometrically caused by a change in the total number of moles of reactant gases before and after reactions. However, there are few studies on the effects of gas volume expansion, and there are many unclear parts about the effects on bubbles. In this study, the effect of the volume expansion of the fluidizing gas on the bed behavior was observed in a two-dimensional (2D) fluidized bed by using the method proposed by Kai et al.[2]. The gas volume expansion was simulated by the evaporation of ethanol impregnated in the pore of porous particles. When the gas volume expands due to reactions, the physical properties of the gas change simultaneously. Therefore, the effect of volume expansion and the effect of gas properties on the fluidization behavior was separately evaluated.

The 2D fluidized bed was made of glass plates coated with transparent heaters to allow heating and visual observation. The height width and depth was 300 mm, 93 mm, and 2 mm, separately. The fluidizing gas was air. The fluidized material was porous alumina particles. The mean size was 61.8 μm and the density was 421 kg/m^3 when they were dried. The pressure drop was measured at the bed bottom using a pressure sensor. Porous particles impregnated with ethanol were fluidized at a temperature higher than room temperature, and the gas volume was expanded by the evaporation of ethanol. Under conditions where the gas volume was not expanded, particles impregnated with glycerin having a boiling point of 563 K were used to obtain the same particle density. The bed being fluidized was photographed with a video camera.

A color image utilizing the difference in porosity as shown in **Fig. 1** was created from a moving image taken by a video camera by image analysis. The image on the right shows a system with an expanding gas volume, and the two on the left show a system with a constant gas volume at the corresponding gas velocity. When the fluidizing gas expanded, the bubble size became a size corresponding to the gas velocity at that height. When the gas volume expands, it is considered that the bubble size reached a size corresponding to the gas velocity as a result of bubble coalescence, splitting, generation and absorption of the gas generated in the emulsion phase. However, when the gas expansion rate was further increased, the equilibrium bubble size was slightly larger than expected from the gas velocity at that height. This is probably because the bubble growth due to gas absorption became predominant over bubble splitting. When the inlet superficial gas velocities were the same, it was expected that the fluidized bed height would also expand because of the increase in bubble hold-up. However, those differences were not observed. Possible causes include that the bubble hold-up was not affected due to the increase in the bubble size and also rising velocity. From the image analysis, we investigated the effect of gas volume expansion on bubble behavior. The effect of gas composition was also investigated by image analysis.

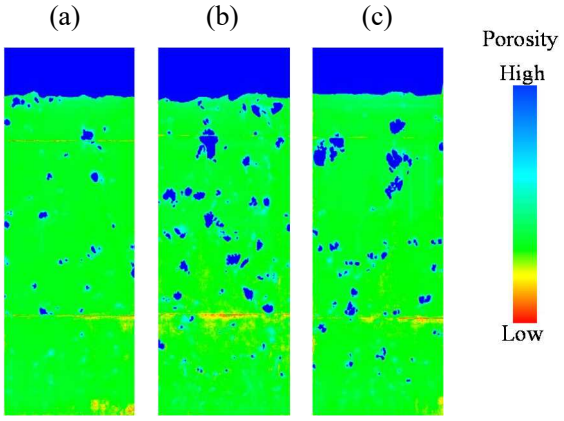

Fig. 1. Fluidization behavior; (a) Constant gas volume (U_G = 1 cm/s), (b) Constant gas volume (U_G = 1.84 cm/s), (c) Gas volume expansion ($U_{G,in}$ = 1 cm/s, $U_{G,out}$ = 1.84 cm/s)

References

1) S. Karimipour, T. Pugsley; "A critical evaluation of literature correlations for predicting bubble size and velocity in gas-solid fluidized beds," *Powder Technol*, **205**, 1-14 (2011)
2) T. Kai, J. Horinouchi, T. Nakazato, T. Tsutsui, T. takahashi and M. Nakajima; "Effects of increase in gas volume on the fluidization properties in fluidized bed reactors," *J. Chem. Eng. Jpn.*, **42**, s137–s141 (2009).

Department of Chemical Engineering, Kagoshima University, Kagoshima 890-0065, Japan

The Twenty-Fifth International Symposium on Artificial Life and Robotics 2020 (AROB 25th 2020),
B-Con Plaza, Beppu, Japan, January 22-24, 2020

A study on reconstructing a 3D model from orthographic views using a satisfiability solver

Yusaku Hayashi[1], Satoshi Ono[1]

Abstract

In the fields of manufacturing, production and design, demand for 3D models has been grown as computer performance has improved, and 3D Computer Aided Design (CAD) systems have been widely used since 1990s. On the other hand, 2D drawings still play an important role as documents that guide product manufacturing and assembly process. Although a lot of software systems including 3D reconstruction function from 2D images have been released on the market, in actual situation, the process of building 3D models is often conducted manually. This is because such tools require many user interactions and only slightly reduces the time of the 3D reconstruction process. Since 1970s, many studies have been conducted for a reconstruction problem, a problem of constructing a 3D model from 2D engineering drawings. However, the reconstruction problem has not been completely solved [1].

Therefore, in this study, the authors propose a 3D reconstruction method that converts the problem to a SAT problem. The proposed method realizes GPU-free and efficient 3D reconstruction by using SAT solver for reconstruction from pseudo wire frame model to surface model. The advantage of the proposed method is easiness of rule addition; it is only necessary to describe a rule as Boolean formula; it does not necessary to design an algorithm that satisfies the rule. In addition, recent SAT solvers have sufficient performance to solve large-scale problems. Experiments with some problem instances demonstrates the effectiveness of the proposed method.

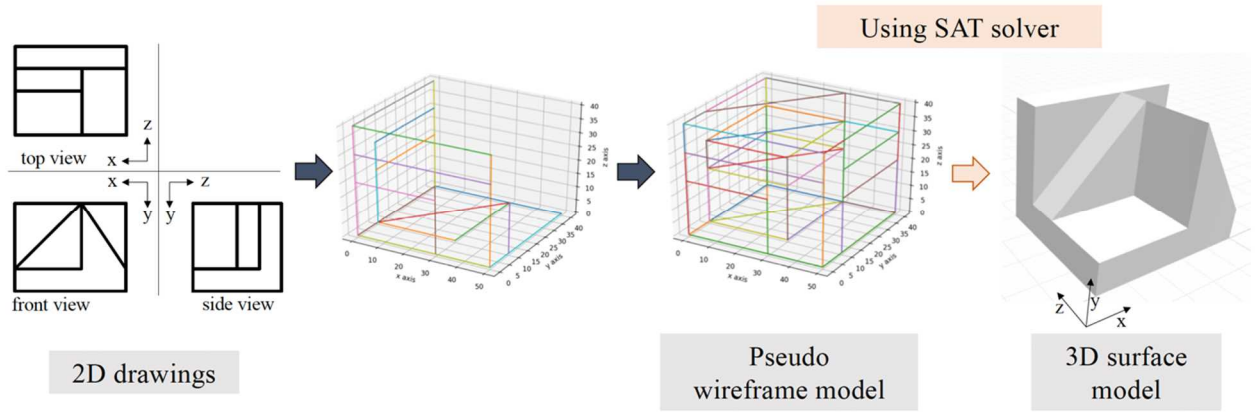

Figure. Overview of the proposed method

References

1. P. Company, A. Piquer, M. Contero, et al. A survey on geometrical reconstruction as a core technology to sketch-based modeling. Computers & Graphics, 2005.

[1] Department of Information Science and Biomedical Engineering, Graduate School of Science and Engineering, Kagoshima University, 890-0065, Kagoshima, Japan

The Twenty-Fifth International Symposium on Artificial Life and Robotics 2020 (AROB 25th 2020),
B-Con Plaza, Beppu, Japan, January 22-24, 2020

Robust adversarial example generation in speech recognition using evolutionary multi-objective optimization

Shoma Ishida[1], Satoshi Ono[1]

Abstract

In recent years, Automatic Speech Recognition (ASR) systems are widely used in many products such as personal assistants of smartphones (e.g. Amazon Alexa and Apple Siri), voice command technologies in cars, and so on. On the other hand, deep learning methods are known to be vulnerable to adversarial examples, a small perturbation added to a target sample. It is essential that ASR systems have high security because ASR systems perform various tasks which may require user personal data. Therefore, studies have been conducted to generate adversarial examples to evaluate and improve the robustness of ASR systems. A few studies attempted to attack the ASR systems under black-box condition where classification result (class labels) and its confidence are available but internal information is not [1]. The black-box attack can be applicable consumer ASR systems and it is expected to find the vulnerabilities of the consumer systems. On the other hand, to discover more serious vulnerabilities in the real world, it is indispensable to design robust perturbations against environmental changes, time gap between the target speech and perturbation, and so on.

Therefore, this paper proposes a method for generating adversarial examples to ASR systems that are robust against time difference because, in the actual environment, it is difficult to play the perturbation noise accurately in time with the target speech. In the proposed method, robust adversarial example design is formulated as a multi-objective optimization problem, and an evolutionary multi-objective optimization algorithm solves the problem. The proposed method can be applicable commercial systems because it assumes the black box setting. Experiments using Speech Commands classification model [6] showed the effectiveness of the proposed method compared to the conventional method in terms of the robustness against the time difference

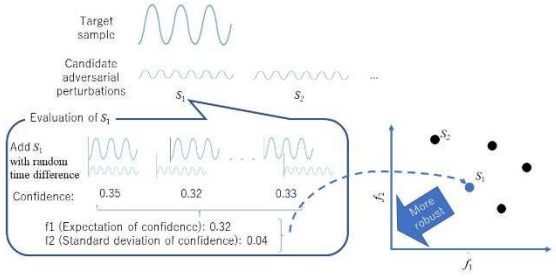

Figure 1. Robust adversarial example generation by multi-objective optimization

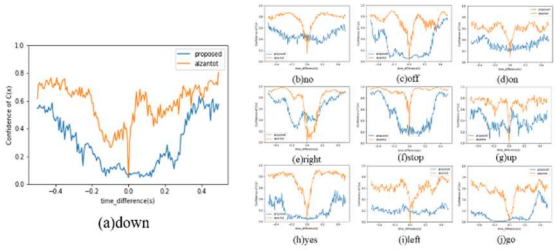

Figure 2. Comparison on the robustness against timing lag.

References

1. M. Alzantot, B. Balaji, M. Srivastava, Did you hear that? adversarial examples against automatic speech recognition, arXiv preprint arXiv:1801.00554 (2018)
2. T. Sainath, C. Parada. Convolutional neural networks for small-footprint keyword spotting, Sixteenth Annual Conference of the International Speech Communication Association (2015).

[1] Department of Information Science and Biomedical Engineering, Graduate School of Science and Engineering, Kagoshima University, 890-0065, Kagoshima, Japan

The Twenty-Fifth International Symposium on Artificial Life and Robotics 2020 (AROB 25th 2020),
B-Con Plaza, Beppu, Japan, January 22-24, 2020

A study on error detection of ocean observation data by anomaly detection

Yosuke Idenoue[1], Shogo Hayashi[2], Ken-ichi Fukui[3],
Shigeki Hosoda[4], and Satoshi Ono[1]

Abstract

Globally-covered ocean monitoring system Argo with more than 3,700 autonomous floats has been working, and its accumulated big ocean observation data helps many studies such as investigation into climate change mechanism. Since the observed data sometimes involves errors, human experts must visually confirm and revise quality control (QC) flags. However, such manual QC by human experts cannot be performed in some countries. In addition, it is difficult to regularize the quality of the ocean observation data of all over the world because the manual QC depends on human experts' heuristics. Therefore, demands have been increasing for automated error detection technologies in Argo observation data.

This paper verifies the validity of the data observed in the sea area other than the North Pacific using the method proposed by Hayashi et al. [Hayashi 18]. Since the method is unsupervised learning, it could be expected to detect unknown errors. Experimental results shown that the method could give a high anomaly score for some error cases. On the other hand, it is difficult to give a high anomaly score to error cases that appeared continuously in multiple layers. Therefore, the method is effective for detecting errors with large fluctuations and appearing on a single layer, and it is difficult to detect errors with minute fluctuations and appearing on multiple layers continuously.

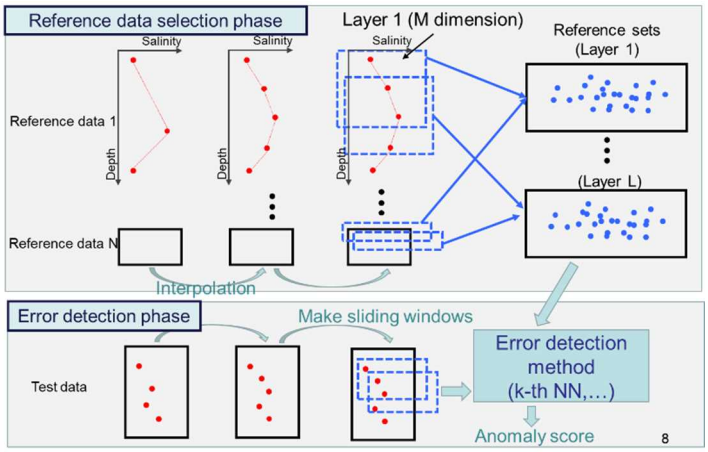

Figure. Overview of the proposed method

References

[Hayashi 18] Shogo Hayashi, Satoshi Ono, Shigeki Hosoda, Masayuki Numao, Ken-ichi Fukui：Error Detection in Ocean Data Considering Spatial Autocorrelation, The Japanese Society for Artificial Intelligence, Vol. 33, (in Japanese)

[1] Department of Information Science and Biomedical Engineering, Graduate School of Science and Engineering, Kagoshima University, Japan
[2] Department of Intelligence Science and Technology, Graduate School of Informatics, Kyoto University, Japan
[3] The institute of Scientific and Industrial Research, Osaka University, Japan
[4] Japan Agency for Marine-Earth Science and Technology, Japan

Study on volatilization and condensation of feed particles in powder-particle Fluidized Bed

Hiroshi Odaka, Tsutomu Nakazato, Takami Kai

Abstract

In the fluidized bed, the reactivity of C particles classified on the Geldart particle classification chart is high. However, when fluidizing using these C particles in a fluidized bed, the C particles are highly sticky and easily form secondary particles, which can cause non-fluidization. Therefore, fluidization with C particles alone is considered difficult.

A powder particle fluidized bed uses fluidized particles with a particle size of several hundreds of μm (B particles) that are easy to fluidize as media particles, and fluidizes while retaining fine particles (C particles) of 40 μm or less on the surface[1]. As a feature of the powder fluidized bed, it is possible to maintain a fluidized state without blowing fine particles to the reaction gas by holding fine particles with strong adhesion/aggregation properties around the medium particles, and collision between the fine particles and the medium particles to prevent the formation of aggregates by destroying the aggregates. Examples of applications include industrialization such as decarbonation of a mixture of silicon carbide and carbon, slurry drying etc.[2]

However, since the zinc produced by the reduction of zinc oxide in this study is a vapor, the fine powder of the raw material changes from solid to gas, condenses in the gas phase, and is recovered as fine powder outside the fluidized bed. Until now, no reaction experiments have been conducted in a granular fluidized bed reactor in which the reactant changes from solid to liquid or gas. Therefore, in this study, as the first study of the reduction of zinc oxide using a granular fluidized bed, we investigated the amount of fines recovered, the chemical form of fine product particles, and the reaction form by temperature for each operating condition, The purpose is to clarify what kind of problems occur in this process.

In this study, the reduction volatilization behavior of zinc oxide was tested using the granular fluidized bed. **Fig. 1** shows the results of the amount of product fine particles scattered at that time. As a result, it can be seen that as the temperature increases, the reaction rate increases and the time until the reduction ends is shortened. In addition, at 5 wt%, the reduction was performed smoothly as the temperature increased, and the amount recovered in the cylindrical filter paper was also high. However, at 10 wt%, the amount recovered was higher at 800℃ than at 850℃. It is conceivable that the condensed zinc of the reduced zinc has increased as a cause of this, and the agglomerated zinc is clogged in the branch pipe. Therefore, it was found that reduction under 10 wt% is optimal under the experimental conditions. Further, at 700℃, condensation and adhesion did not occur in the quartz tube and the branch tube, and almost no reduction reaction occurred, so it was found that the reduction starting temperature was about 760℃.

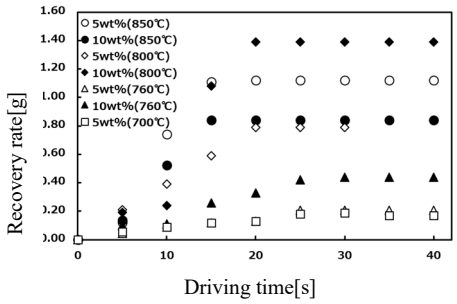

Fig. 1 Recovery ratio of product fine particles with time

Next, **Fig. 2** shows the particle size distribution of the recovered fine particles in the cylindrical filter paper at 5 wt%, U_{mf}, 50% H_2-50% N_2 at temperatures of 760℃, 800℃, and 850℃. From the results in Fig. 3, it was confirmed that the recovered product was recovered in the form of fine particles. It can also be seen that the average particle size of the recovered particles decreases with increasing temperature. The reason is that when the temperature rises, the ZnO oxide film is destroyed by the reduction reaction.

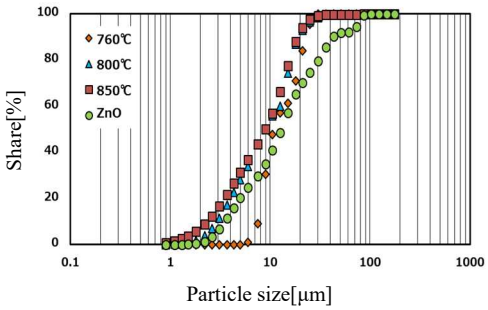

Fig. 2 Changes in particle size distribution of reactant ZnO powder and product powder after reduction in PPFB

References

1) K.Kato: "Behavior of Fine Particle in Powder Particle Fluidized Bed," *J. Soc. Power Technol., Japan*, **36**, 613-619 (1999)

2) T. Nakazato; "Recent developments in fluidized bed technology (in Japanese)," *Ryudosogijutsuno Saikinno Shinten*, pp.33-41, Kagaku Kogyosha (2008)

Department of Chemical Engineering, Kagoshima University, Kagoshima 890-0065, Japan